Applied Thermal Engineering 284 (2026) 129116

Contents lists available at ScienceDirect

Applied Thermal Engineering

journal homepage: www.elsevier.com/locate/apthermeng

Research Paper

Diamond/Cu composites microchannel heat sink for effective thermal management of SiC power devices

Kangyong Li [a], Rong Zhang [a], Kai Yang [b], Haoran Shen [b], Jialiang Chen [c], FanFan Wang [a], Jian Huang [a], Zexin Liu [d], Yue Yue [d], Zhiqiang Wang [b], Guoqing Xin [a,*]

[a] Wuhan National High Magnetic Field Center and School of Materials Science & Engineering and State Key Laboratory of High Density Electrical Energy Conversion, Huazhong University of Science and Technology, Wuhan 430074, China
[b] School of Electrical and Electronic Engineering, Huazhong University of Science and Technology, Wuhan 430074, China
[c] School of Physics, Huazhong University of Science and Technology, Wuhan 430074, China
[d] School of Chemistry and Chemical Engineering, Huazhong University of Science and Technology, Wuhan 430074, China

ARTICLE INFO

Keywords:
Diamond/Cu composites
Microchannel
Heat sinks
Thermal management
Power device

ABSTRACT

SiC power devices offer higher efficiency and power density than their Si counterparts but suffer from severe heat-dissipation challenges that conventional Cu or Al heat sinks cannot meet. Diamond/Cu composites provide ultrahigh thermal conductivity, yet their application is limited by interfacial thermal resistance and the difficulty of machining into precise cooling structures. Here, we simultaneously overcome these two bottlenecks by fabricating a diamond/Cu composite microchannel heat sink: a high-conductivity diamond/Cu composite baseplate (807 W/m·K) was achieved via W-coated diamond particles and vacuum annealing to minimize interfacial resistance, and precise Cu microchannels were integrated by active-metal brazing to realize efficient convective cooling. Infrared thermography and thermal-resistance measurements reveal a 39 % reduction in thermal resistance compared with an all-Cu counterpart, while SiC module testing shows a 12.3 °C lower peak junction temperature at 200 W. This work demonstrates a practical integration of interface-engineered diamond/Cu composites with microchannel cooling, offering a scalable route toward advanced thermal management of high-power electronics.

1. Introduction

Wide-bandgap devices like silicon carbide (SiC) have attracted significant attention as they are able to work at higher breakdown voltage, lower switching losses and higher operating frequency compared with silicon (Si)-based devices [1]. The reduced SiC chip size enables higher power density for the packaged modules, however, leading to higher heat flux and elevated junction temperature [2]. In SiC power devices, long-term operation at high temperatures leads to substantial failures, mainly due to the malfunction of packaging components [3]. Examples of such failures include bond wire lift-off [4], substrate delamination [5], die-attach cracks [6] and degradation of encapsulation materials [7]. Furthermore, multi-chips in parallel connection become an inevitable approach to increase the device's current capacity due to the limited flow of the individual chips [8]. The asymmetric layouts and mismatched chip parameters result in unbalanced currents, leading to mismatched power losses and non-uniform junction temperatures of the parallel chips [9]. The mismatched thermomechanical stress of the parallel chips further degrades the reliability and stability of the SiC devices [10]. Consequently, the thermal management challenges associated with the high-power density SiC devices have emerged as a critical factor restricting device reliability and lifespan [11].

Several cooling methods have been explored to address the overheating issues of high power density devices, including jet impingement cooling [12,13], spray cooling [14,15], microchannel cooling [16–18] and thermoelectric cooler cooling [19,20]. Among these cooling techniques, microchannel cooling shows promising performances due to its compact structure and high heat transfer coefficient [21]. By optimizing the microchannel structure, the temperature of electronics with high heat flux has been well-controlled [22]. For instance, Sarvey *et al.* [23] optimized the shape and arrangement of the fins in the microchannel heat sink to enhance the cooling performance for an integrated circuit. Similarly, Drummond *et al.* [24] applied hierarchical manifold microchannels to successfully control the temperature of a 0.2 × 0.2 mm^2

* Corresponding author.
E-mail address: guoqingxin@hust.edu.cn (G. Xin).

https://doi.org/10.1016/j.applthermaleng.2025.129116
Received 16 June 2025; Received in revised form 3 November 2025; Accepted 11 November 2025
Available online 12 November 2025

hotspot below 130 °C through optimizing the aspect ratio. These literatures reports indicate the great potential of microchannel cooling in dealing with high heat flux in SiC devices [25]. In the realm of power device thermal management, Cu and Al are the commonly employed materials for heat sinks, with thermal conductivities of 398 W/m·K and 270 W/m·K, respectively. Given the soft nature of Cu and Al, microchannel heat sinks are predominantly fabricated by skiving thick Cu or Al baseplates, with the channel width capable of scaling down to approximately 200 μm. However, the through-plane thermal resistance of the thick Cu and Al baseplate becomes a bottleneck, especially as SiC chip areas shrink and device-level heat fluxes can reach 500 W/cm^2 [26]. As a result, the heat conduction capabilities of traditional Cu and Al heat sinks are no longer adequate to meet the heat dissipation requirements of SiC devices, motivating higher-thermal-conductivity thermal management materials.

Diamond/Cu composites combine high thermal conductivity with a low coefficient of thermal expansion (CTE), showing great promise in addressing the overheating problems of SiC power devices [27–29]. However, the raw-diamond/pure-Cu composite owns weak interfacial bonding, and the phonon scattering at the interface is pretty serious, resulting in the actual thermal conductivity being far inferior to the theoretical value [30]. For example, Ma et al. acquired the commercial Ti-coated diamond particles (prepared by magnetron sputtering) and hot-forged into a pancake Cu/diamond composite, but the diamond/Cu composites was revealed that the thermal conductivity of the composite was only 350 W/m·K [31]. In other reports, Ishida et al. [32] have utilized electroplating to achieve 595 W/m·K and Constantin et al. [33] employing 3D printing technology to achieve 330 W/m·K. According to the interfacial phonon mismatch theory model (AMM) and the differential medium effective model (DEM), the acoustic properties of the interfacial layer determine the thermal conductivity of the composites by affecting the interfacial thermal conductivity [34]. Besides, Yang et al. [35] used Molecular Dynamics to study the interfacial thermal conductance of diamond copper composites. They reported that the acoustic differences between diamond and copper are the main reason for low interfacial thermal conductance. Without careful interface engineering, the effective thermal conductivity of diamond/Cu composites can be significantly limited relative to that of their constituents [36]. Thus, the engineering of interfaces becomes crucial in the development of diamond/Cu composite thermal management materials [37]. One approach is to add reactive elements(e.g., Zr [38,39], Cr [40–42], B [43,44], or Ti [45,46]) into the Cu matrix so that they diffuse to the diamond surface and form a carbide interlayer that improves interfacial bonding and interfacial thermal conductivity [47]. Exceptional thermal conductivities exceeding 900 W/m·K have been reported by gas pressure infiltration with Cu alloy to achieve a better interface. However, high diamond loadings (60–81 vol%)[48,49] and melted copper at high temperature are typically empolyed, which entail higher costs and complexity. Besides, it should be noted that the dissolution of the alloying elements into the Cu matrix inevitably degrades its thermal conductivity [50]. Therefore, researchers prefer to use diamond surface metallization to introduce the interface layer [51]. Coating diamond with a carbide layer or pure metals can further improve the thermal properties of composites by mitigating the negative effects of alien elements in the Cu matrix [52]. Ti [53], Cr [54], W [55–57], Mo [58], and Zr [59] layers have been coated onto the diamond surface to enhance the interfacial bonding effectively. Several coating methods have been reported, such as ion plating [60], magnetron sputter deposition [36], and the molten salt method [61]. Compared to other diamond coating techniques, direct current (DC) magnetron sputtering technology was an ambient-temperature coating approach that did not harm the diamond during the deposition process [62]. However, additional heat treatment is generally required to increase their interface bonding force, leading to more complicated steps in diamond pretreatment [63]. Besides, reported thermal conductivities of diamond/Cu composites still deviate substantially from theoretical predictions, largely because the coating layers are difficult to control in terms of composition, thickness, and stability [64]. Consequently, achieving a coating that is both well-bonded and thermally efficient remains a bottleneck for realizing the full potential of diamond/Cu composites.

Furthermore, diamond's remarkable hardness brings significant challenges to machine diamond/Cu composites into a precise-shaped structure. Conventional machining methods such as laser engraving and CNC struggle to mill diamond/Cu composites into efficient heat dissipation structures such as microchannels. Therefore, other more flexible processing techniques need to be combined to prepare diamond/Cu composite materials into fine heat dissipation structures. For example, Wu et al. [65] fabricated micro pin fins structure with diamond/Cu composites (450 W/m·K) via electroplated method, and Zhang et al. [66] three-dimensionally printed diamond/Cu composites via selective laser melting (336 W/m·K). However, these methods were unable to fully exploit the advantages of diamond/Cu composites' high thermal conductivity. This manufacturability bottleneck remains the main obstacle preventing diamond/Cu composites from being widely deployed in high-power electronics.

In this study, diamond/Cu composites microchannel heat sinks have been fabricated by actively brazing Cu microchannels and diamond/Cu plates, and applied for SiC devices cooling. A diamond/Cu baseplate with high thermal conductivity up to 807 W/m·K has been prepared by the optimization of the interface between diamond particles and Cu. Skived Cu microchannels were then integrated with the diamond/Cu baseplate using active metal brazing to obtain the final heatsink. Benefited from the high thermal conductivity, diamond/Cu microchannel heatsinks exhibited a 39 % reduction in thermal resistance compared to the traditional Cu microchannel heatsinks with the same dimensions. The diamond/Cu microchannel heatsinks have been employed as the direct cooling baseplate for the SiC power devices. Under the same coolant flow and power input, the peak junction temperature of the SiC device with diamond/Cu microchannel heatsink shows a 12.3 °C reduction compared to that of the SiC device with Cu microchannel heatsink. This research thus offers a promising solution for the effective thermal management of SiC power devices.

2. Experimental

2.1. Preparation of the diamond/Cu composites

High-purity synthetic single-crystal diamond particles (HWD-40 grade, 70/80 mesh; Henan Huanghe Whirlwind Co., Ltd., China) and gas-atomized Cu powder (99.99 % purity, 25–50 μm particle size distribution; Zhongye Xindun Alloy Co., Ltd., China) were employed as starting materials. Owing to the intrinsically low thermal boundary conductance (TBC) between diamond and Cu, which is arising from atomic-structure and phonon-spectrum mismatches [67], surface pretreatment of diamond particles is carried out by a two-step metallization process: first, metallic tungsten (W) was deposited on the diamond surface by magnetron sputtering, and then vacuum annealed in a tube furnace at a temperature of 1000 °C for 1 h. This process can induce the formation of a uniform WC transition layer on the diamond surface, thereby enhancing the interfacial bonding strength between the diamond particles and Cu [68].

The diamond/Cu composites microchannel heat sink was fabricated through a three-step process, as illustrated in Fig. 1(a). First, W-coated diamond particles were uniformly blended with Cu powder. Second, the mixture was consolidated by vacuum hot-press sintering in a graphite mold at 1000 °C, 50 MPa, for 3 h [53], and the specific t profile for the sintering process is shown in Fig. 1(b). This parameter set was chosen based on literature for high-volume-fraction diamond/metal composites [37,69,70], where 1000 °C ensures sufficient Cu-matrix softening for densification and a 40–60 MPa window provides strong interparticle contact without damaging the mold. In our trials, 50 MPa consistently achieved > 95 % theoretical density and high thermal conductivity,

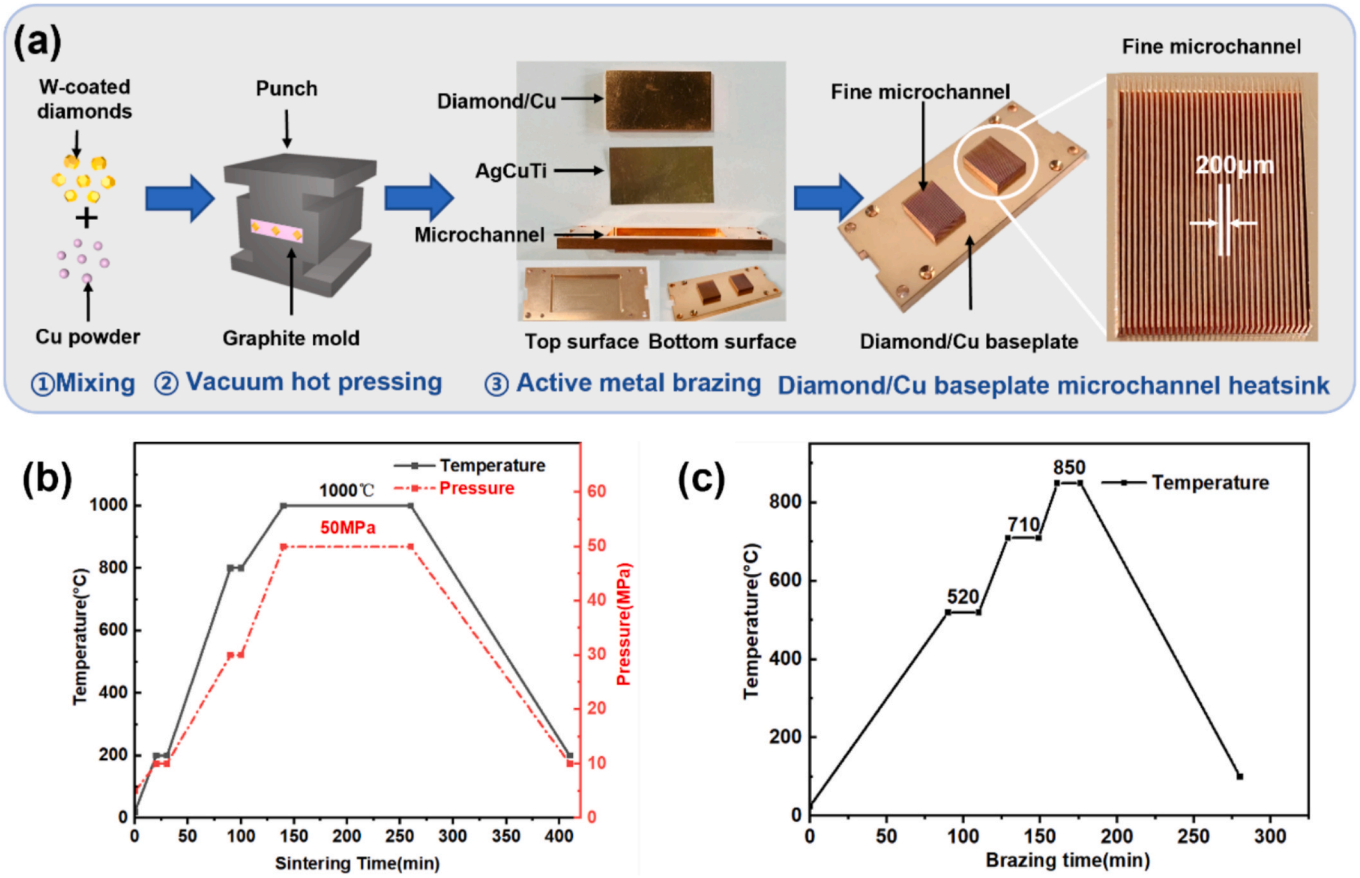

Fig. 1. Schematic illustration of the fabrication process for the diamond/Cu baseplate microchannel heatsink. (a) Three-step manufacturing protocol including mixing W-coated diamonds and Cu powder, vacuum hot pressing, and active metal brazing; (b) Temperature–pressure profile used for vacuum hot pressing; (c) Heating profile applied during active metal brazing with AgCuTi.

whereas pressures < 40 MPa left residual porosity and > 60 MPa often fractured graphite molds, increasing experimental and production costs. A 3 h dwell allowed adequate interfacial reaction and near-full densification. Finally, the sintered diamond/Cu baseplate was joined to precision-machined Cu microchannels (200 μm width) via active-metal brazing using an AgCuTi filler. The brazing parameters (heating curve in Fig. 1(c)) were selected to balance filler wettability, minimal thermal damage to the composite, and void-free bonding—based on prior vacuum-bra2zing studies for dissimilar materials [71,72] and verified by preliminary bonding trials in this work. This method yielded a high-thermal-conductivity microchannel heat sink with a robust metallurgical bond between the diamond/Cu baseplate and the Cu microchannels, ensuring efficient thermal management performance.

2.2. Characterization

The surface morphology of diamond particles and interfacial bonding characteristics of diamond/Cu composites were analyzed using scanning electron microscopy (SEM, Thermo Fisher Scientific, Scios 2). Elemental distribution of W-coated diamond was examined by energy dispersive X-ray spectroscopy (EDS, Oxford Instruments, Ultim Max 40). Composites density was measured via a high-precision solid densitometer (DK-600A, DECCA, China) based on Archimedes' principle. The relative density (D) of the composites can be calculated by the following Eq. (1) [60]:

$$D = \frac{\rho_c}{\rho_l} \times 100\% \quad (1)$$

where ρ_c represents the measured density of diamond/Cu composites, and ρ_l denotes the theoretical density derived from rule-of-mixtures calculations.

The thermal diffusivity of diamond/Cu composites at room temperature was determined through laser flash analysis (LFA467 Hyper Flash, NETZSCH, Germany). Specimens with standardized dimensions (3 mm thickness × 12.7 mm diameter) underwent triplicate measurements under identical conditions. The thermal diffusivity coefficient was measured three times and obtained by averaging the three values. To ensure the consistency of the thermal radiation emissivity on the surface, the samples were carbon-sprayed before the test. The density ρ_c of the composites material was measured by a densitometer, and the specific heat capacity C_p of the sample was calculated based on the mass fractions of diamond and Cu in the composites. The thermal conductivity (λ) of the composites material can be calculated by the following Eq. (2) [73]:

$$\lambda = \alpha \times C_p \times \rho_c \quad (2)$$

where α represents the measured thermal diffusivity.

3. Results and discussion

3.1. Microstructural characterization

Low thermal boundary conductance (TBC) exhibits between Cu and diamond, which arises from the fundamental mismatches in their atomic structures and vibrational properties and hinders efficient phonon-mediated heat transfer across the interface [67]. To address this interfacial incompatibility, a strategic approach involving diamond surface metallization was implemented to establish W-based interfacial

architectures [74]. Fig. 2 presents the surface morphology of diamond particles before and after depositing W coating. The uncoated diamond particles have sharp edges and smooth surfaces, which are typical of their natural crystallographic structure (Fig. 2(a)). Fig. 2(b) shows SEM photographs of diamond particles uniformly covered with a layer of W on the surface after magnetron sputtering. Fig. 2(c) presents a high-magnification SEM image of the W-coated diamond surface. The coating appears uniform and continuous, with an estimated average thickness of approximately 122.4 nm, as measured from the cross-sectional profile. The EDS elemental maps in Fig. 2(d-f) offer additional information about the chemical composition of the coated particles. Specifically, the uniform distribution of W in Fig. 2(e) confirms an even deposition of the W layer on all crystallographic planes of the diamond particles.

To further enhance interfacial bonding, high-temperature annealing was carried out to promote carbide formation. XRD analysis (Fig. 2(g)) shows that before annealing, the coating is primarily metallic W. After annealing at 1000 °C for 1 h, the intensity of W peaks decreases, while reflections corresponding to WC emerge. The diffraction peaks can be indexed to standard cards: diamond (JCPDS 06–0675) and WC (JCPDS 25–1047), confirming the generation of a thin carbide interlayer [57]. XPS analysis (Fig. 2(h)) provides further evidence of this phase evolution. The deconvoluted W 4f spectrum reveals characteristic peaks of metallic W, WC, and W_2C. These findings confirm that part of the W coating transforms into carbides during annealing. The coexistence of W and carbide phases indicates that a well-bonded interfacial layer is established. Importantly, the carbide thickness remains limited (~122.4 nm), which provides strong adhesion without introducing excessive interfacial thermal resistance [75]. Overall, the combined SEM, EDS, XRD, and XPS results demonstrate that controlled W metallization and annealing lead to a uniform W/WC/W_2C interfacial architecture. This structure effectively balances interfacial bonding strength and phonon transport, thereby facilitating high thermal conductivity in the diamond/Cu composites.

Fig. 3 presents the fractured characteristics of W-coated diamond/Cu composites. The selected diamond/Cu was synthesized under optimized processing parameters of 1000 °C for 3 h under 50 MPa uniaxial pressure with a volume ratio of 55 % diamond and 45 % Cu powder. The SEM image demonstrates homogeneous dispersion of diamond reinforcements within the Cu matrix (Fig. 3(a)). Multi-scale analysis (Fig. 3(a-b)), combining low-magnification imaging and high-resolution microscopy, reveals the critical interfacial feature of the absence of debonding cracks at diamond/Cu interfaces. This microstructural evolution confirms the effectiveness of the tungsten carbide transition layer in establishing metallurgical bonding at the diamond-Cu interface. The observed pore-free interface morphology, particularly the intimate contact region shown in Fig. 3(b), significantly reduces phonon scattering at phase boundaries – a critical prerequisite for achieving enhanced thermal transport properties in particle-reinforced metal matrix composites [76].

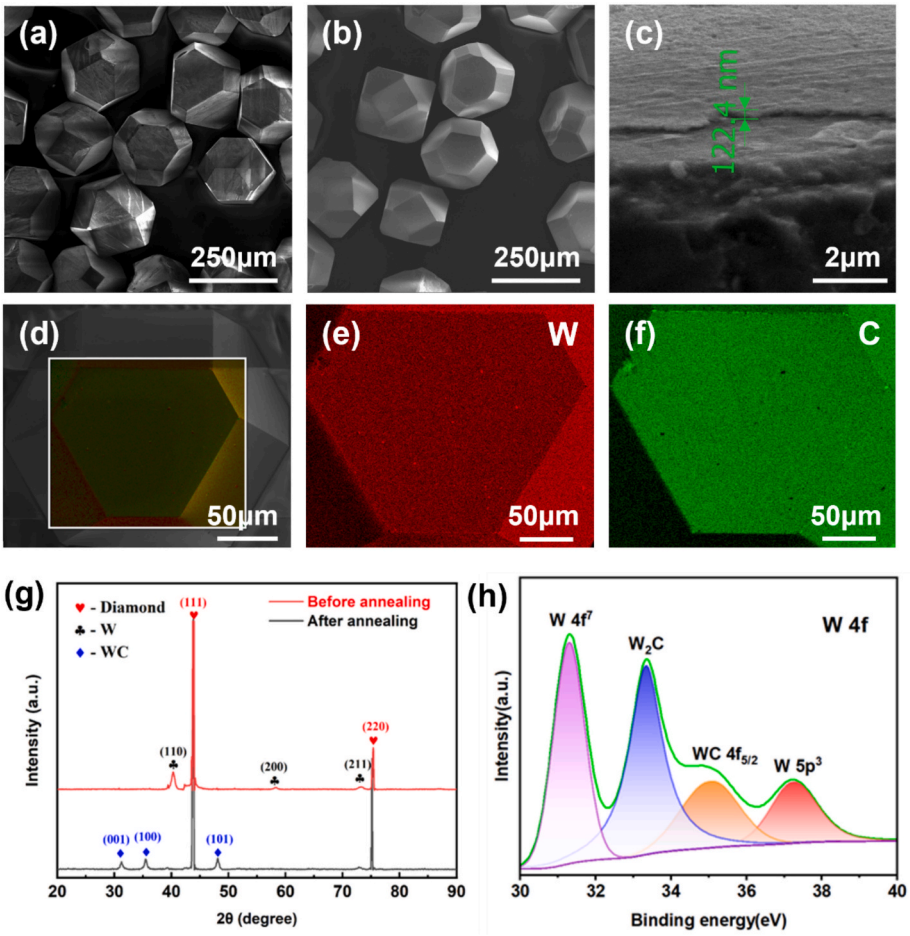

Fig. 2. SEM images and EDS elemental mapping, XRD and XPS analysis of diamond particles with and without W coating. (a) Surface morphology of pristine diamond particles, (b) Surface morphology of W-coated diamond particles, (c) Highly magnified image of W-coating; (d) EDS analysis of the magnified area of W-coated diamond particle, (e, f) EDS mapping distribution of W (e) and C (f). (g) XRD patterns of W-coated diamond before and after annealing, (h) XPS spectra of W 4f.

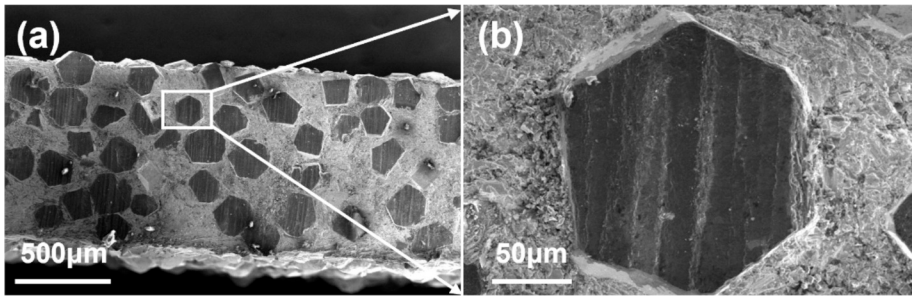

Fig. 3. Fractured morphology of the diamond/Cu composites prepared by vacuum hot-press sintering at different magnifications. (a) The cross-sectional view of the diamond/Cu plate, (b) Enlarged view of diamond particles tightly embedded in Cu without pin-holes.

3.2. *Thermal performance of the diamond/Cu composites*

The thermal conductivity and heat spreading performance of diamond/Cu composites were thoroughly evaluated and compared with pure Cu baseplates, as shown in Fig. 4. The thermal conductivity and relative density of diamond/Cu composites with different diamond volume fractions are given in Fig. 4(a). It can be seen that the thermal conductivity reaches a maximum value of 807 W/m·K when the diamond volume fraction is increased to 55 %. The thermal conductivity decreases slightly at a higher diamond filling fraction of 60 %, which may be caused by the incomplete sintering densification due to the increase in the contact interface between the matrix and the reinforcing phase, at which point the relative density decreases to 97 % [77]. Fig. 4 (b) gives photographs of a diamond/Cu composites baseplate and a Cu baseplate, both with nickel-plated surfaces. A heat source was placed on the lower surface of the baseplate, and an infrared thermographic camera was used to detect the temperature distribution on the upper surface of the heatsink baseplate, as shown in Fig. 4(c), and the temperature measurement curves are shown in Fig. 4(d). The heating rate of the diamond/Cu baseplate is higher than that of the Cu baseplate under

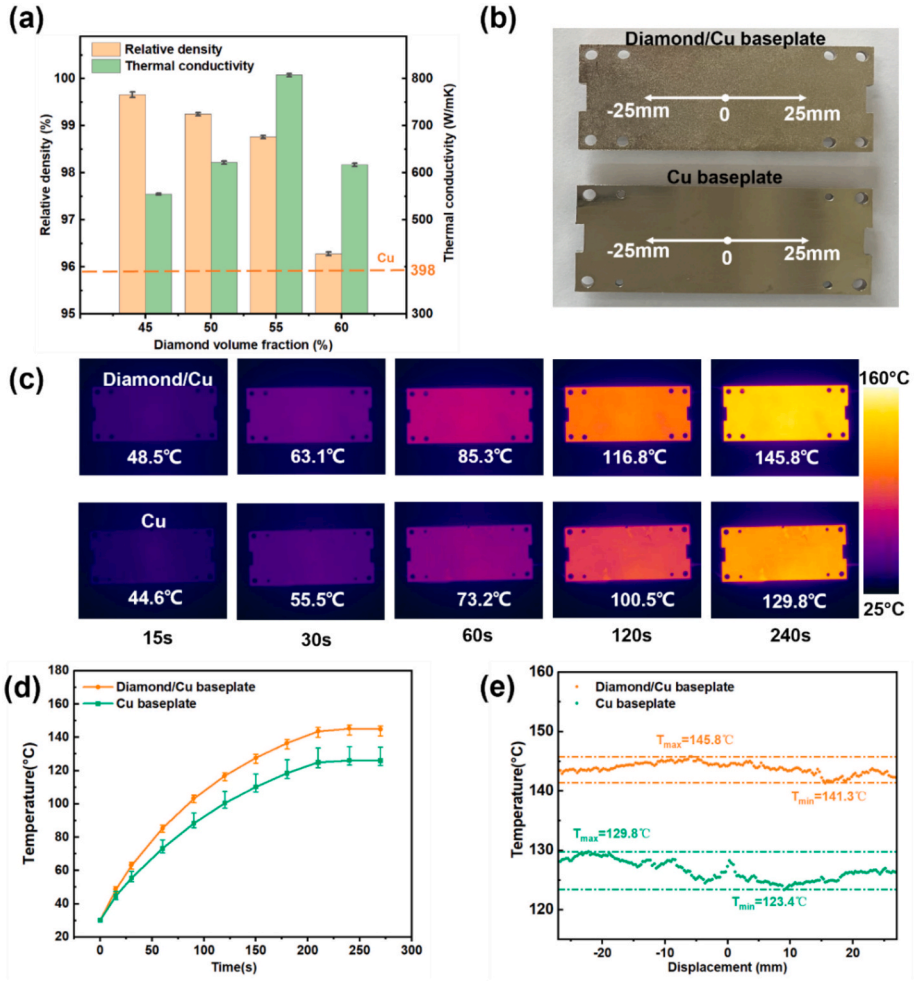

Fig. 4. Thermal performance of the diamond/Cu composites. (a)Thermal conductivities and relative densities of diamond/Cu composites with different diamond volume fractions; (b) Photograph of the diamond/Cu baseplate and the Cu baseplate with electroplated nickel finishing; (c) Infrared thermal images of surface of different baseplate; (d) Average surface temperature of two types of baseplates versus time; (e) Temperature profiles along the long axis centerline of the baseplates at 240 s.

the same heating conditions. When the heating time reaches 240 s, the steady state temperature of the diamond/Cu baseplate is 145.8 °C, which is 16 °C higher than that of the Cu baseplate, indicating that the heat transfer performance of the diamond/Cu baseplate is superior to that of the Cu baseplate along the vertical direction. Fig. 4(e) shows the temperature distribution curves along the centerline of the diamond/Cu and Cu heatsink baseplates at steady state. After statistical analysis, we can get the maximum temperature difference ($T_{max} - T_{min}$) along the centerline of the diamond/Cu baseplate is 4.5 °C, and the standard deviation is 0.9622, which is lower than that of the pure Cu baseplate by 29.69 % and 41.85 %, respectively, indicating that the diamond/Cu baseplate has a better heat dispersion capability along the lateral direction.

3.3. Microchannel heat sink thermal resistance measurements

A diamond/Cu microchannel heatsink was assembled by joining the highly thermally conductive diamond/Cu composites with a skived Cu microchannel heatsink. To assess the quality and effectiveness of the brazing process, the diamond/Cu microchannel heatsink was inspected and analyzed in three dimensions using X-ray imaging. It can be seen that the surface of the assembled diamond/Cu microchannel heatsink is clean, smooth and well-defined, with no visible solder swell or accumulation. Moreover, no significant voids were found inside the heatsink, indicating that the diamond/Cu microchannel heatsink is tightly brazed. Fig. 5(b) illustrates the schematic diagram of the experimental setup used to measure the thermal resistance of the microchannel heatsinks. This setup was designed to ensure uniformity during thermal performance testing, with the thermocouple positioned 2 mm from the centerline of the heat source's long axis. Fig. 5(c) compares the surface temperature rise of the diamond/Cu heatsink and the pure Cu heatsink at different heating power levels. The results demonstrate that the surface temperature rise of the diamond/Cu heatsink is significantly lower than that of the Cu heatsink at all tested power levels. Specifically, when the heating power increased to 200 W, the surface temperature rise of the Cu heatsink is approximately 11.4 °C, while the surface temperature rise of the diamond/Cu heatsink was only 7.1 °C.

The above results comprehensively demonstrate that the diamond/Cu heatsink has a more efficient heat dissipation capability compared to the conventional Cu heatsink. The following equation can be used to calculate the thermal resistance of the microchannel heatsink to further quantify this heat dissipation performance [78]:

$$R = \frac{T_h - Tc}{P} \tag{3}$$

where T_h is the maximum temperature of heatsink surface[79], T_c is the temperature of water temperature at the inlet[80], P is the heating power [81].

Fig. 5(d) presents a comparison of thermal resistance between the two heatsinks under varying heating powers. The Diamond/Cu heatsink consistently exhibits lower thermal resistance than the Cu counterpart, demonstrating the enhanced heat dissipation efficiency of the composites material. At a heating power of 200 W, the diamond/Cu heatsink achieves thermal resistance of 0.035 K/W, which is 39 % lower than the 0.057 K/W measured for the Cu heatsink. This significant reduction in thermal resistance highlights the superior thermal conductivity of the diamond/Cu composites, thereby optimizing the overall heat dissipation performance of the microchannel heatsink.

3.4. Thermal performance of SiC power device with diamond/Cu heat sink

The SiC power device was assembled using the developed diamond/Cu composites microchannel heatsink. Nano-silver paste is employed as the solder material to integrate the DBC substrate, SiC MOSFET, and diamond/Cu microchannel heatsink, as illustrated in Fig. 6(a). Fig. 6(b) displays the X-ray transmission image of the SiC device, demonstrating robust bonding between the diamond/Cu microchannel heatsink, SiC MOSFET, and DBC substrate, with no visible voids or defects. Fig. 6(c) shows a photograph of the complete SiC power device. Finite element simulations are further performed to compare the thermal performance of the SiC power device integrated with the diamond/Cu heatsink (Fig. 6 (d)) and the standard Cu heatsink (Fig. 6(e)). Under identical cooling

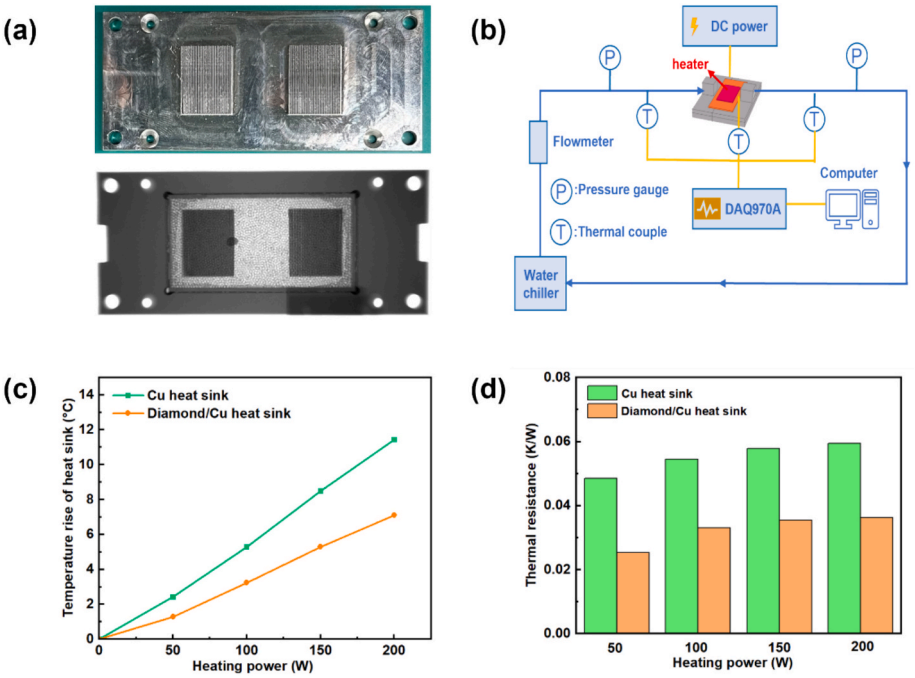

Fig. 5. Thermal resistance measurements of microchannel heatsink. (a) Photograph and X-ray transmission image of diamond/Cu heatsink; (b) Schematic diagram of the thermal resistance measurement setup for the microchannel heatsink; (c) Comparison of the temperature rise on the heatsink surface; (d) Comparison of the thermal resistance.

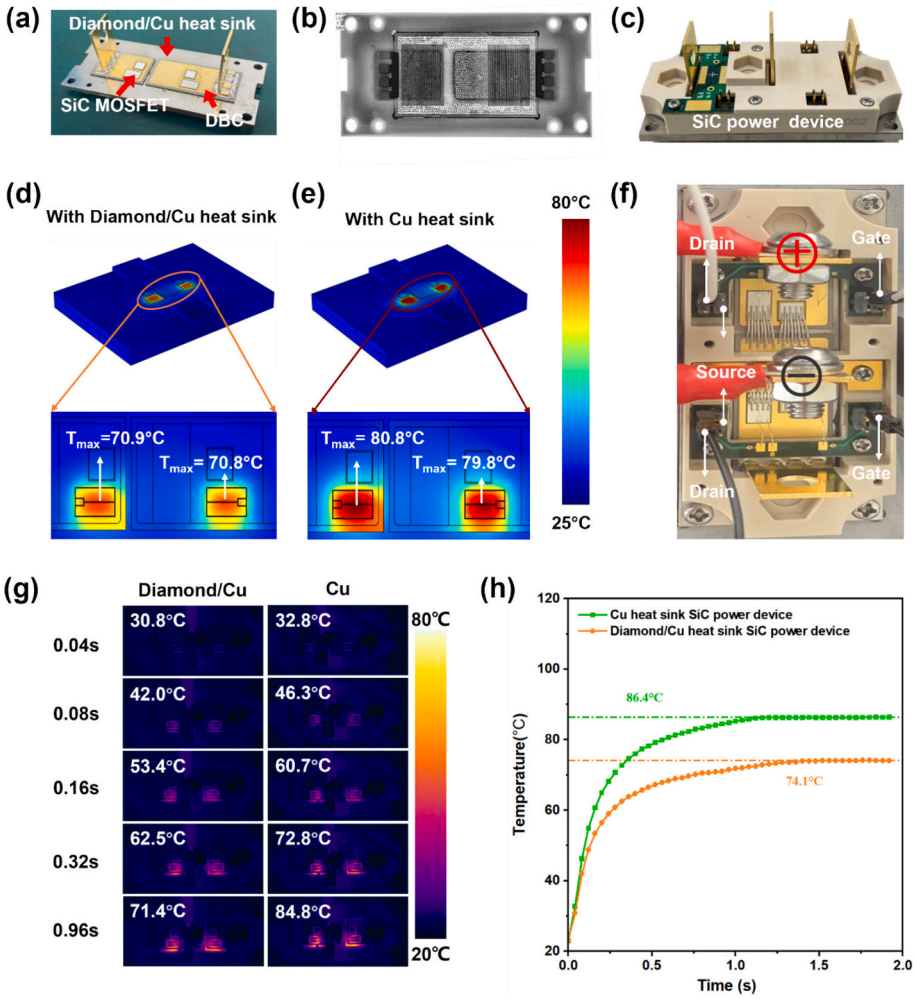

Fig. 6. Thermal performance evaluation of SiC power device integrated with the diamond/Cu composites heatsink. (a) Photograph of the SiC MOSFET chip sintered onto the diamond/Cu heatsink using nanosilver paste; (b) X-ray image after chip sintering; (c) Photograph of the fully assembled SiC power device package; (d) Simulated temperature distribution of the power device using the diamond/Cu heatsink; (e) Simulated temperature distribution of the power device using a conventional Cu heatsink (f) Schematic diagram of electrode layout and wire bonding configuration; (g) Infrared thermal images of the power device using different heatsinks under identical operating conditions; (h) Junction temperature of the power device as a function of time for different heatsink materials.

conditions (chip power: 200 W, coolant flow rate: 4 L/min), the maximum junction temperature of a device equipped with the diamond/Cu heatsink reaches 70.9 °C, significantly lower than that of the Cu-based SiC device (80.8 °C). The results confirm that the diamond/Cu microchannel heatsink significantly enhances the thermal management capability of SiC power devices, enabling their stable operation under high-power-density conditions. In order to capture the surface temperature of SiC chips, no sealant was applied to the SiC device (Fig. 6(f)). Under this configuration, the gate and drain are short-circuited and the two Cu rows are connected to the DC power supply in order to generate heat. Fig. 6(g) presents infrared thermal images of the power devices equipped with two different heatsinks. The surface temperature of the device equipped with a diamond/Cu microchannel heatsink reaches only 71.4 °C, while the device with the Cu heatsink reaches a higher temperature of 84.8 °C during the initial operation. This indicates that the diamond/Cu microchannel heatsink provides superior heat-dissipating capability. The junction temperature rise curves in Fig. 6 (h) further highlight the heat removal advantages of the diamond/Cu heatsink. The steady-state junction temperature of the diamond/Cu heatsink is approximately 74.1 °C, significantly lower than the 86.4 °C recorded for the device with Cu heatsink. Additionally, during the initial heating phase, the surface temperature of the SiC power device with the Cu heatsink rises more rapidly, while the device with the diamond/Cu heatsink experiences a more gradual increase. This difference helps to effectively reduce the thermal stress on the SiC power device during operation.

The improved thermal performance of the SiC power device with the diamond/Cu microchannel heatsink can be attributed to the superior thermal conductivity and uniform heat distribution of the diamond/Cu composites. The lower junction temperature and more even temperature distribution enhance the reliability and efficiency of the SiC power device. These findings highlight the potential of diamond/Cu composites for high-power electronic applications, where effective thermal management is essential.

4. Conclusion

In summary, this study addresses two long-standing bottlenecks that have limited the practical use of diamond/Cu composites for thermal management: weak interfacial bonding that suppresses conductivity, and poor machinability that prevents integration into efficient cooling structures. By combining W-coated diamond particles with vacuum annealing, we obtained a diamond/Cu baseplate of 807 W/m·K demonstrating effective interface engineering. Through active-metal brazing of skived Cu microchannels, we further overcame the manufacturability challenge and realized a composite microchannel heat sink

capable of device-level operation. Infrared thermography and thermal-resistance testing confirmed a 39 % reduction in thermal resistance compared with an all-Cu counterpart, while SiC module integration achieved a 12.3 °C reduction in peak junction temperature at 200 W. These results not only validate the dual approach of interface optimization and structural integration but also establish a scalable route to exploit the intrinsic advantages of diamond/Cu composites for advanced thermal management in SiC devices and beyond.

CRediT authorship contribution statement

Kangyong Li: Writing – review & editing, Writing – original draft, Methodology, Investigation, Formal analysis, Data curation, Conceptualization. **Rong Zhang:** Writing – review & editing. **Kai Yang:** Formal analysis. **Haoran Shen:** Investigation. **Jialiang Chen:** Investigation. **FanFan Wang:** Data curation. **Jian Huang:** Investigation. **Zexin Liu:** Data curation. **Yue Yue:** Investigation. **Zhiqiang Wang:** Supervision. **Guoqing Xin:** Writing – review & editing, Methodology, Funding acquisition, Conceptualization.

Declaration of competing interest

The authors declare that they have no known competing financial interests or personal relationships that could have appeared to influence the work reported in this paper.

Acknowledgments

This work was supported by the Key Program of National Natural Science Foundation of China (No. U24B20100). The authors appreciate the Analytical and Testing Center of Huazhong University of Science and Technology (HUST) for SEM, EDS and LFA testing.

Appendix A. Supplementary data

Supplementary data to this article can be found online at https://doi.org/10.1016/j.applthermaleng.2025.129116.

Data availability

The data that support the findings of this study are available from the corresponding author upon reasonable request.

References

[1] Y. Zhang, T. Palacios, (Ultra)Wide-bandgap vertical power FinFETs, IEEE Trans. Electron Devices 67 (2020) 3960–3971.
[2] L. Zhang, X. Yuan, X. Wu, C. Shi, J. Zhang, Y. Zhang, Performance evaluation of high-power SiC MOSFET modules in comparison to Si IGBT modules, IEEE Trans. Power Electron. 34 (2019) 1181–1196.
[3] H. Lee, V. Smet, R. Tummala, A review of SiC power module packaging technologies: challenges, advances, and emerging issues, IEEE J. Emerg. Select. Topic. Power Electron. 8 (2020) 239–255.
[4] P. Ning, R. Lai, D. Huff, F. Wang, K.D.T. Ngo, V.D. Immanuel, K.J. Karimi, SiC wirebond multichip phase-leg module packaging design and testing for harsh environment, IEEE Trans. Power Electron. 25 (2010) 16–23.
[5] R. Khazaka, L. Mendizabal, D. Henry, R. Hanna, Survey of high-temperature reliability of power electronics packaging components, IEEE Trans. Power Electron. 30 (2015) 2456–2464.
[6] S. Fu, Y. Mei, X. Li, C. Ma, G.Q. Lu, Reliability evaluation of multichip phase-leg IGBT modules using pressureless sintering of nanosilver paste by power cycling tests, IEEE Trans. Power Electron. 32 (2017) 6049–6058.
[7] J. Chen, T. Luo, H. Huang, L. Zhang, W. Chen, G. Qin, J. Fan, H. Zeng, Glass-based encapsulant enabling SiC power devices to long-term operate at 300 °C, Appl. Surf. Sci. 680 (2025) 161452.
[8] Y. Yan, J. Lv, B. Liu, Y. Zhang, J. Liu, C. Chen, Y. Kang, Multichip parallel double-sided cooling silicon carbide power module with low parasitic inductance and balanced dynamic current, IEEE J. Emerg. Select. Top. Power Electron. 12 (2024) 4596–4611.
[9] Z. Zheng, C. Chen, J. Lv, Y. Yan, J. Liu, Y. Kang, A Dynamic current Sharing Model of Multichip Parallel SiC MOSFETs considering Layout-Dominated Mutual Inductance Coupling, IEEE Trans. Power Electron. 39 (2024) 11060–11073.
[10] C. Chen, F. Luo, Y. Kang, A review of SiC power module packaging: Layout, material system and integration, CPSS Trans. Power Electron. Appl. 2 (2017) 170–186.
[11] C. Zhao, L. Wang, F. Zhang, Effect of Asymmetric Layout and Unequal Junction Temperature on current Sharing of Paralleled SiC MOSFETs with Kelvin-Source connection, IEEE Trans. Power Electron. 35 (2020) 7392–7404.
[12] S. Sarkar, R. Gupta, T. Roy, R. Ganguly, C.M. Megaridis, Review of jet impingement cooling of electronic devices: emerging role of surface engineering, Int. J. Heat Mass Transf. 206 (2023) 123888.
[13] B. Yang, S. Chang, H. Wu, Y. Zhao, M. Leng, Experimental and numerical investigation of heat transfer in an array of impingement jets on a concave surface, Appl. Therm. Eng. 127 (2017) 473–483.
[14] Y. Hu, Y. Lei, X. Liu, R. Yang, Heat transfer enhancement of spray cooling by copper micromesh surface, Mater. Today Phys. 28 (2022) 100857.
[15] J. Feng, W. Chen, P. Tan, C. Liu, H. Wang, F. Du, Experimental study on heat-transfer characteristics of spray cooling for microchannel radiators, Appl. Therm. Eng. 245 (2024) 122913.
[16] C. Hu, X. Yang, Z. Ma, X. Ma, Y. Feng, J. Wei, Research on heat transfer and flow distribution of parallel-configured microchannel heat sinks for arrayed chip heat dissipation, Appl. Therm. Eng. 255 (2024) 124003.
[17] S. Yang, J. Li, B. Cao, Z. Wu, K. Sheng, Investigation of Z-type manifold microchannel cooling for ultra-high heat flux dissipation in power electronic devices, Int. J. Heat Mass Transf. 218 (2024) 124792.
[18] D. Zhuang, Y. Yang, G. Ding, X. Du, Z. Hu, Optimization of Microchannel Heat Sink with Rhombus Fractal-like units for Electronic Chip Cooling, Int. J. Refrig 116 (2020) 108–118.
[19] H.H. Saber, S.A. AlShehri, W. Maref, Performance optimization of cascaded and non-cascaded thermoelectric devices for cooling computer chips, Energ. Conver. Manage. 191 (2019) 174–192.
[20] Z.-G. Chen, W.-D. Liu, Thermoelectric coolers: Infinite potentials for finite localized microchip cooling, Journal of Materials Science & Technology 121 (2022) 256–262.
[21] X. Zhang, Z. Ji, J. Wang, X. Lv, Research progress on structural optimization design of microchannel heat sinks applied to electronic devices, Appl. Therm. Eng. 235 (2023) 121294.
[22] D. Lorenzini, Y. Joshi, Flow boiling heat transfer in silicon microgaps with multiple hotspots and variable pin fin clustering, Phys. Fluids 31 (2019) 102002.
[23] T.E. Sarvey, Y. Hu, C.E. Green, P.A. Kottke, D.C. Woodrum, Y.K. Joshi, A. G. Fedorov, S.K. Sitaraman, M.S. Bakir, Integrated circuit cooling using heterogeneous micropin-fin arrays for nonuniform power maps, IEEE Trans. Compon. Packag. Manuf. Technol. 7 (2017) 1465–1475.
[24] K.P. Drummond, D. Back, M.D. Sinanis, D.B. Janes, D. Peroulis, J.A. Weibel, S. V. Garimella, Characterization of hierarchical manifold microchannel heat sink arrays under simultaneous background and hotspot heating conditions, Int. J. Heat Mass Transf. 126 (2018) 1289–1301.
[25] Z.-Q. Yu, M.-T. Li, B.-Y. Cao, A comprehensive review on microchannel heat sinks for electronics cooling, Int. J. Extreme Manufactur. 6 (2024) 022005.
[26] E. Laloya, L.Ó.H. Sarnago, J.M. Burdío, Heat management in power converters: from state of the art to future ultrahigh efficiency systems, IEEE Trans. Power Electron. 31 (2016) 7896–7908.
[27] W. He, J. Zhang, R. Guo, C. Pei, H. Li, S. Liu, J. Wei, Y. Wang, Performance analysis and structural optimization of a finned liquid-cooling radiator for chip heat dissipation, Appl. Energy 327 (2022) 120048.
[28] Y. Xia, L. Chen, J. Luo, W. Tao, Numerical investigation of microchannel heat sinks with different inlets and outlets based on topology optimization, Appl. Energy 330 (2023) 120335.
[29] L. Lou, Z. Kang, H. Zhang, P. Wang, J. Fan, Nano-capillary aluminum finned heat sink for ultra-efficient evaporative cooling, Mater. Today Phys. 36 (2023) 101175.
[30] C.A. Polanco, R. Rastgarkafshgarkolaei, J. Zhang, N.Q. Le, P.M. Norris, A. W. Ghosh, Design rules for interfacial thermal conductance: Building better bridges, Phys. Rev. B 95 (2017) 195303.
[31] J.N. Ma, L. Bolzoni, F. Yang, Interface manipulation and its effects on the resultant thermal conductivity of hot-forged copper/Ti-coated diamond composites, J. Alloy. Compd. 868 (2021) 159182.
[32] N. Ishida, K. Kato, N. Suzuki, K. Fujimoto, T. Hagio, R. Ichino, T. Kondo, M. Yuasa, H. Uetsuka, A. Fujishima, C. Terashima, Preparation of amino group functionalized diamond using photocatalyst and thermal conductivity of diamond/copper composite by electroplating, Diam. Relat. Mater. 118 (2021) 108509.
[33] L. Constantin, L. Fan, M. Pontoreau, F. Wang, B. Cui, J.-L. Battaglia, J.-F. Silvain, Y. F. Lu, Additive manufacturing of copper/diamond composites for thermal management applications, Manuf. Lett. 24 (2020) 61–66.
[34] G.T. Hohensee, R.B. Wilson, D.G. Cahill, Thermal conductance of metal–diamond interfaces at high pressure, Nat. Commun. 6 (2015) 6578.
[35] K. Yang, Z. Zhang, H. Zhao, B. Yang, B. Zhong, N. Chen, J. Song, C. Chen, D. Tang, J. Zhu, Y. Liu, T. Fan, Orientation independent heat transport characteristics of diamond/copper interface with ion beam bombardment, Acta Mater. 220 (2021) 117283.
[36] J. Jia, S. Bai, D. Xiong, J. Wang, J. Chang, Effect of tungsten based coating characteristics on microstructure and thermal conductivity of diamond/Cu composites prepared by pressueless infiltration, Ceram. Int. 45 (2019) 10810–10818.
[37] W. Chen, F. Wang, L. Fan, H. Zheng, X. Guo, P. Zheng, L. Zheng, Y. Zhang, Double layer interfacial structure of Cr3C2–Cr7C3 in copper/diamond composites for thermal management applications, Appl. Therm. Eng. 255 (2024) 123958.

[38] L. Wang, J. Li, G. Bai, N. Li, X. Wang, H. Zhang, J. Wang, M.J. Kim, Interfacial structure evolution and thermal conductivity of Cu-Zr/diamond composites prepared by gas pressure infiltration, J. Alloy. Compd. 781 (2019) 800–809.
[39] H. Zhang, Y. Qi, J. Li, J. Wang, X. Wang, Effect of Zr Content on Mechanical Properties of Diamond/Cu-Zr Composites Produced by Gas pressure Infiltration, J. Mater. Eng. Perform. 27 (2018) 714–720.
[40] Z. Xie, H. Guo, X. Zhang, S. Huang, H. Xie, X. Mi, Tailoring the thermal and mechanical properties of diamond/Cu composites by interface regulation of Cr alloying, Diam. Relat. Mater. 114 (2021) 108309.
[41] L. Wang, J. Li, L. Gao, X. Wang, K. Xu, H. Zhang, J. Wang, M.J. Kim, Gradient interface formation in Cu–Cr/diamond(Ti) composites prepared by gas pressure infiltration, Vacuum 206 (2022) 111549.
[42] L. Wang, J. Li, Z. Che, X. Wang, H. Zhang, J. Wang, M.J. Kim, Combining Cr pre-coating and Cr alloying to improve the thermal conductivity of diamond particles reinforced Cu matrix composites, J. Alloy. Compd. 749 (2018) 1098–1105.
[43] G. Bai, L. Wang, Y. Zhang, X. Wang, J. Wang, M.J. Kim, H. Zhang, Tailoring interface structure and enhancing thermal conductivity of Cu/diamond composites by alloying boron to the Cu matrix, Mater Charact 152 (2019) 265–275.
[44] G. Bai, Y. Zhang, W. Shi, X. Wang, H. Zhu, F. Wang, H. Zhang, Investigation of the matrix and interface of Cu–B/diamond composite by atom probe tomography, Ceram. Int. 50 (2024) 12915–12923.
[45] L. Yang, L. Sun, W. Bai, L. Li, Thermal conductivity of Cu-Ti/diamond composites via spark plasma sintering, Diam. Relat. Mater. 94 (2019) 37–42.
[46] Z. Deng, J. Lu, H. Li, Y. Wu, X. Xu, Q. Miao, W. Zhang, First-principles study on adhesive work, electronic structures and mechanical properties of Cr/Ti-doped Cu (100)/diamond(100) interfaces, Diam. Relat. Mater. 151 (2025) 111861.
[47] L. Zhou, J. Liu, R. Ding, J. Cao, K. Zhan, B. Zhao, A review of diamond interfacial modification and its effect on the properties of diamond/Cu matrix composites, Surf. Interfaces 40 (2023) 103143.
[48] J. Li, X. Wang, Y. Qiao, Y. Zhang, Z. He, H. Zhang, High thermal conductivity through interfacial layer optimization in diamond particles dispersed Zr-alloyed Cu matrix composites, Scr. Mater. 109 (2015) 72–75.
[49] J. Hao, Y. Zhang, N. Li, J. Dai, X. Wang, H. Zhang, Synergetic effect enabling high thermal conductivity in Cu/diamond composite, Diam. Relat. Mater. 138 (2023) 110213.
[50] A. Rape, X. Liu, A. Kulkarni, J. Singh, Alloy development for highly conductive thermal management materials using copper-diamond composites fabricated by field assisted sintering technology, J. Mater. Sci. 48 (2013) 1262–1267.
[51] L. Chen, S. Chen, Y. Hou, Understanding the thermal conductivity of Diamond/Copper composites by first-principles calculations, Carbon 148 (2019) 249–257.
[52] C. Wang, H. Li, M. Chen, Z. Li, L. Tang, Microstructure and thermo-physical properties of CuTi double-layer coated diamond/Cu composites fabricated by spark plasma sintering, Diam. Relat. Mater. 109 (2020) 108041.
[53] H. Li, Y. Xie, L. Zhang, H. Wang, Thermal properties of diamond/Cu composites enhanced by TiC plating with molten salts containing fluoride and electroless-plated Cu on diamond particles, Diam. Relat. Mater. 129 (2022) 109337.
[54] X. Liu, F. Sun, L. Wang, Z. Wu, X. Wang, J. Wang, M.J. Kim, H. Zhang, The role of Cr interlayer in determining interfacial thermal conductance between Cu and diamond, Appl. Surf. Sci. 515 (2020) 146046.
[55] J. Wang, X. Wang, J. Gu, R. Ding, S. Xu, W. Chen, H. Zheng, X. Guo, P. Zheng, L. Zheng, Y. Zhang, Interfacial engineering in diamond/cu composites: from W-WC single-layer optimization to WCu dual-layer Interface for high-temperature thermal properties and stability, Diam. Relat. Mater. 156 (2025) 112408.
[56] W. Chen, J. Qian, S. Peng, L. Fan, H. Zheng, Z. Zhang, P. Zheng, L. Zheng, Y. Zhang, Thermal properties of tungsten/tungsten carbide-coated double-size diamond/copper composite, Diam. Relat. Mater. 135 (2023) 109818.
[57] W. Dou, C. Zhu, X. Wu, X. Yang, W. Fa, Y. Zhang, J. Tong, G. Zhu, Z. Zheng, Lightweight diamond/Cu interface tuning for outstanding heat conduction, Carbon Energy 5 (2023) e379.
[58] R. Liu, G. Luo, Y. Li, J. Zhang, Q. Shen, L. Zhang, Microstructure and thermal properties of diamond/copper composites with Mo2C in-situ nano-coating, Surf. Coat. Technol. 360 (2019) 376–381.
[59] L. Wang, G. Bai, N. Li, L. Gao, J. Li, K. Xu, X. Wang, H. Zhang, J. Wang, M.J. Kim, Unveiling interfacial structure and improving thermal conductivity of Cu/diamond composites reinforced with Zr-coated diamond particles, Vacuum 202 (2022) 111133.
[60] H. Sun, L. Guo, N. Deng, X. Li, J. Li, G. He, J. Li, Elaborating highly thermal-conductive diamond/Cu composites by sintering intermittently electroplated core-shell powders, J. Alloy. Compd. 810 (2019) 151907.
[61] H. Li, Y. Xie, H. Wang, Z. Qian, P. Cao, W. Zhang, Facile formation of a thin chromium carbide coating on diamond particles via quaternary molten salt, J. Alloy. Compd. 928 (2022) 167142.
[62] X. Xu, B. Wan, W. Li, F. Liu, T. Zhai, L. Zhang, G. Tang, Reaction mechanisms for Ti coatings on diamond, Carbon 226 (2024) 119206.
[63] Z. Yan, W. Tong, X. Wang, D. Fan, A review of diamond composites for heat spreaders, Compos. A Appl. Sci. Manuf. 196 (2025) 109008.
[64] K. Chu, Z. Liu, C. Jia, H. Chen, X. Liang, W. Gao, W. Tian, H. Guo, Thermal conductivity of SPS consolidated Cu/diamond composites with Cr-coated diamond particles, J. Alloy. Compd. 490 (2010) 453–458.
[65] Y. Wu, L. Lai, Y. Wang, Z. Yang, H. Wang, G. Ding, Micro Heat Sink Structure with High Thermal Conductive Composite via Micromachining Process, in: 2019 20th International Conference on Solid-State Sensors, Actuators and Microsystems & Eurosensors XXXIII (TRANSDUCERS & EUROSENSORS XXXIII), 2019, pp. 1776-1779.
[66] L. Zhang, Y. Li, S. Li, P. Gong, Q. Chen, H. Geng, M. Sun, Q. Sun, L. Hao, Fabrication of Titanium and Copper-Coated Diamond/Copper Composites via Selective Laser Melting, in: Micromachines, Vol. 13, 2022, pp. 724.
[67] G. Chang, F. Sun, L. Wang, Z. Che, X. Wang, J. Wang, M.J. Kim, H. Zhang, Regulated interfacial thermal conductance between Cu and diamond by a TiC interlayer for thermal management applications, ACS Appl. Mater. Interfaces 11 (2019) 26507–26517.
[68] J. Jia, S. Bai, D. Xiong, J. Xiao, T. Yan, Enhanced thermal conductivity in diamond/copper composites with tungsten coatings on diamond particles prepared by magnetron sputtering method, Mater. Chem. Phys. 252 (2020) 123422.
[69] C. Wang, H. Li, M. Chen, Z. Li, L. Tang, Microstructure and thermo-physical properties of Cu Ti double-layer coated diamond/Cu composites fabricated by spark plasma sintering, Diam. Relat. Mater. 109 (2020) 108041.
[70] Z. Xie, H. Guo, Z. Zhang, X. Zhang, Thermal expansion behaviour and dimensional stability of Diamond/Cu composites with different diamond content, J. Alloy. Compd. 797 (2019) 122–130.
[71] N.Y. Taranets, H. Jones, Wettability of AlN with different roughness, porosity and oxidation state by commercial Ag-Cu-Ti brazes, J. Mater. Sci. 40 (2005) 2355–2359.
[72] J.-W. Peng, F.-L. Zhang, Y.-M. Zhou, L.-K. Xiong, Y.-J. Huang, H.-Q. Tang, Fabrication of diamond/copper composite thin plate based on a single-layer close packed diamond particles network for heat dissipation, Chem. Eng. J. 476 (2023) 146666.
[73] G. Chang, S. Zhang, K. Chen, W. Zhang, L. Li, Y. Zhang, H. Peng, D. Kan, L. Wang, H. Zhang, W. Huo, Achieving excellent thermal transport in diamond/Cu composites by breaking bonding strength-heat transfer trade-off dilemma at the interface, Compos. B Eng. 289 (2025) 111925.
[74] J. Sang, L. Zhou, W. Yang, J. Zhu, L. Fu, D. Li, Enhanced thermal conductivity of copper/diamond composites by fine-regulating microstructure of interfacial tungsten buffer layer, J. Alloy. Compd. 856 (2021) 157440.
[75] Y. Zhang, Z. Wang, N. Li, Z. Che, X. Liu, G. Chang, J. Hao, J. Dai, X. Wang, F. Sun, H. Zhang, Interfacial thermal conductance between Cu and diamond with interconnected W-W2C interlayer, ACS Appl. Mater. Interfaces 14 (2022) 35215–35228.
[76] S. Cui, F. Sun, D. Wang, X. Zhang, H. Zhang, Y. Feng, Enhancing interfacial heat conduction in diamond-reinforced copper composites with boron carbide interlayers for thermal management, Compos. B Eng. 287 (2024) 111871.
[77] K. Lu, C. Wang, C. Wang, H. He, X. Fan, F. Chen, F. Qi, Study of the hot-pressing sintering process of diamond/copper composites and their thermal conductivity, J. Alloy. Compd. 960 (2023) 170608.
[78] D. Ansari, K.-Y. Kim, Hotspot thermal management using a microchannel-pinfin hybrid heat sink, Int. J. Therm. Sci. 134 (2018) 27–39.
[79] X. Hao, B. Liu, Y. Li, J. Zhao, S. Zhang, D. Wen, K. Liu, B. Dai, J. Han, J. Zhu, Diamond single crystal-polycrystalline hybrid microchannel heat sink strategy for directional heat dissipation of hot spots in power devices, Diam. Relat. Mater. 135 (2023) 109858.
[80] D. Ansari, J.H. Jeong, A silicon-diamond microchannel heat sink for die-level hotspot thermal management, Appl. Therm. Eng. 194 (2021) 117131.
[81] D. Ansari, K.Y. Kim, Performance analysis of double-layer microchannel heat sinks under non-uniform heating conditions with random hotspots, Micromachines 8 (2017) 54.